Contactless electrical impedance and ultrasonic tomography: correlation, comparison and complementarity study

OPEN ACCESS
IOP Publishing
Measurement Science and Technology
Meas. Sci. Technol. **30** (2019) 114001 (10pp)
https://doi.org/10.1088/1361-6501/ab2292

Contactless electrical impedance and ultrasonic tomography: correlation, comparison and complementarity study

Yandan Jiang[1], **Manuchehr Soleimani**[2] **and Baoliang Wang**[1]

[1] State Key Laboratory of Industrial Control Technology, College of Control Science and Engineering, Zhejiang University, Hangzhou, People's Republic of China
[2] Department of Electronic and Electrical Engineering, Engineering Tomography Laboratory (ETL), University of Bath, Bath, United Kingdom

E-mail: M.Soleimani@bath.ac.uk and wangbl@zju.edu.cn

Received 10 January 2019, revised 30 April 2019
Accepted for publication 17 May 2019
Published 21 August 2019

Abstract

Electrical tomography (ET) and ultrasonic tomography (UT) techniques are effective and promising super-sensing tools with uses in many industrial process applications. They can create internal mapping images of both electrical and mechanical properties from measurements at the exterior boundaries of domains of interests. There are several different types of ET methods and different modes of UT imaging. Here we focus on contactless ET and contactless UT imaging for liquid masses, enabling fully non-intrusive, integrated mechanical and electrical imaging because direct contact to the process material is often a major limiting factor. ET is sensitive to the distribution of dielectric parameters inside the region of interest, and the highest sensitivity often lies near the outer surface of the boundary. UT has very good responses to the intersections of different phases of materials and has the highest resolution in the central area. Capacitively coupled electrical impedance tomography (CCEIT) is proposed as a contactless ET technique. This work investigates CCEIT based on phase measurements of the electrical impedance between transmitting and receiving electrodes, and UT based on the transmission mode, measuring the time-of-flight between the transmitted signal and the first received signals. A combined sensor which comprises a 16-electrode CCEIT array and a 16-transducer UT array is developed. Experimental results show the performances of the two tomography systems and their dual modality combination. This work highlights various aspects of the correlation, comparison and complementarity between these two contactless imaging techniques. Inclusion material characterization and identification is demonstrated using this novel dual modality.

Keywords: capacitively coupled electrical impedance tomography (CCEIT), phase measurement, ultrasonic tomography (UT), transmission mode, contactless imaging, dual-modality

(Some figures may appear in colour only in the online journal)

1. Introduction

Tomography has been used in process industry for decades and is now a very popular imaging technology for multi-component media inside industrial pipes and vessels, including gas–liquid, liquid–liquid, liquid–solid and gas–solid media [1–4]. Although there are many tomography types and modalities available, none of them is a universal choice able to image all kinds of processes [4–6]. Overall, electrical tomography (ET) and ultrasonic tomography (UT) are among the most widely applied modalities. However, due to different sensing mechanisms, they show different characteristics.

ET is a soft-field tomography technique which is sensitive to the dielectric property inside the region of interest (ROI) [7, 8]. It has highest sensitivity near the boundary of a ROI but very low sensitivity in the central area. Electrical impedance tomography (EIT) is one kind of ET which has gained much attention from researchers in both the process and medical tomography fields since it was proposed [9–15]. It can non-intrusively reveal the distribution of electrical impedance inside a ROI, and it has many advantages such as its low cost, high speed and radiation-free character [9–11].

UT is to some extent a hard-field tomography technique. It has the highest resolution in the centre and relatively poor resolution near the boundary of a ROI [16, 17]. It is able to reconstruct the spatial distribution of acoustic impedance ($Z_c = \rho c$, where ρ and c are, respectively, the density of the media and the velocity of sound), which cannot easily be obtained by other methods [16–18]. UT can perform non-invasive measurement, so it has been successfully applied in chemical and industrial processes, especially in flow measurement [19, 20]. Although UT has very good response to intersections between different phases and can provide useful information about the shape and size of the disperse phase inside the continuous background, the low boundary resolution limits its practical applications.

As more and more industrial processes are highly complex and contain multiple components, effective combination of complementary modalities is preferred to obtain better tomographic performance [21–28]. Currently, UT is a good choice to complement other tomographic imaging techniques such as EIT. In recent decades, much research has been undertaken and valuable achievements and knowledge have been obtained. Soleimani discussed the combination of ultrasound and EIT information [21]. Results showed that the EIT reconstruction was faster and more accurate when using the additional edge information from an ultrasound system. Yunus *et al* combined UT and ERT for imaging of two-phase gas–liquid flow, and simulation results showed good detection resolution of 10 mm gas bubbles in a 100 mm diameter acrylic vessel, with the simulated optimum ERT electrode size [22]. Samir Teniou *et al* presented a new ERT-UT system for automatic exploration of soft tissues, using good localization information of some edge points provided by UT to improve the image resolution obtained by ERT [23]. Steiner *et al* and Ain *et al* separately proposed dual-modality EIT with ultrasound reflection (EIT-UR) to produce high resolution and contrast imaging in the medical field, and results indicated considerable improvement of image quality [24, 25]. Tan *et al* studied the combination of ultrasonic transducers operated in continuous Doppler mode for flow velocity measurement and a conductance sensor (UTCC) for phase fraction measurement to estimate the individual flow velocities in oil–water two-phase flows [26]. Liang *et al* used a direct position measurement of two ultrasonic transducers as the prior information for guiding an EIT-based free-interface reconstruction to improve the spatial resolution of EIT [27].

All these works obtained meaningful advancements and make useful references. However, the proposed combinations are based on the traditional EIT sensor, a contact measurement method, and will bring some negative influences on measurement during practical applications [3]. For example, the electrochemical erosion effect, polarization effect and contamination of the electrodes will cause measurement errors. To overcome the above negative sides of traditional EIT, capacitively coupled electrical resistance tomography (CCERT) was proposed as a new contactless EIT by Wang *et al* [29, 30]. This idea provides a good reference for contactless impedance imaging. As such, research on combinations of UT and contactless capacitively coupled EIT (CCEIT) should be carried out to implement a totally contactless combination. In addition, most EIT research works use only the real part of measurements for conductivity imaging (including the novel CCEIT) or use the real/imaginary part for separate conductivity/permittivity imaging [6, 31, 32]. In many cases, however, it is not possible to describe the physical quantities by either permittivity or conductivity alone but only by using a combination of the two. As the combination of the real part and the imaginary part, the phase information of the impedance reveals the complex internal interplay of the two parts and may provide some additional information. So, more attention should be paid to the phase information of the impedance [33].

This work aims to study the individual performances of phase-based CCEIT and ultrasonic transmission tomography (UTT), and to show the correlation, comparison and complementarity of these two contactless tomography techniques. In addition, combination of the images obtained separately by the two modalities is also implemented. The possibilities of further combination and dual-modality system development are discussed.

2. Measurement principle

2.1. Capacitively coupled electrical impedance tomography (CCEIT)

Figure 1(a) shows the construction of a 16-electrode CCEIT sensor, including 16 electrodes, an insulating pipe and the conductive medium inside the pipe. Sixteen electrodes are mounted equidistantly outside the insulating pipe and the electrodes are not in contact with the conductive medium. Between every electrode and the conductive background in the ROI, a coupling capacitance will be generated via the insulating pipe. So, for each measurement electrode pair, the two electrodes (one excitation electrode and one detection electrode), the

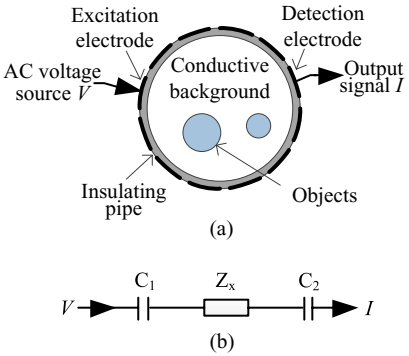

Figure 1. Measurement principle of CCEIT. (a) Construction. (b) Equivalent circuit of a measurement electrode pair.

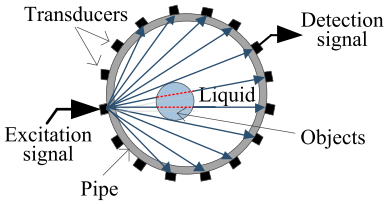

Figure 2. Measurement principle of UTT.

insulating pipe, and the conductive medium will form two coupling capacitances, making contactless measurement possible [29]. The conductive medium can be regarded as an impedance. Figure 1(b) shows the equivalent circuit of an electrode pair, where C_1 and C_2 are the two coupling capacitances and Z_x is the impedance of the medium between the two electrodes. When an AC voltage source V is applied to the excitation electrode, an output signal I, which contains the information of Z_x, can be obtained on the detection electrode. Here, the phase information of Z_x is used for imaging.

In a whole measurement cycle (i.e. the cycle to obtain an image), there will be 120 independent impedance measurements. Numbering the electrodes from 1 to 16, first, electrode 1 is selected as the excitation electrode and electrodes 2–16 are selected as the detection electrode one by one. Then, electrode 2 is excited and measurement can be obtained from electrode 3–16 in turn. We proceed until electrode 15 and 16 are selected as the measurement electrode pair. For every measurement, except for the two selected electrodes, the other electrodes are kept at floating potential to make the model in figure 1(b) valid.

2.2. Ultrasonic transmission tomography (UTT)

Figure 2 shows a 16-transducer UT sensor. The imaged object(s) inside the liquid background is surrounded by 16 transducers. The transducers are fixed to the outer periphery of the pipe/tank, which means they are totally contactless. When one transducer emits an ultrasonic field, the other transducers can record the transmitted or reflected/scattered ultrasonic signals from various directions [18, 34]. The ultrasonic wave is strongly reflected on the interface between materials with a great difference in acoustic impedance. However, it is difficult to collimate as the enclosed pipe/vessel wall will cause reflections, as well [35].

In this work, the UT transmission mode and the fan beam projection method are adopted, i.e. only the transmission signal is used for imaging. In UTT, the amplitude or time-of-flight (TOF) measurement of the received wave is used for imaging based on the assumption of straight-line propagation [20, 36]. As an ultrasonic signal propagates with different speeds in different materials, the material distribution inside the ROI can influence its straight-line propagation time, which is termed as TOF. According to this statement, imaging can be implemented by measuring the TOF of ultrasonic signals between transducers, which is the UT methodology utilized in this work. Meanwhile, the fan-shaped ultrasonic beam projection allows simultaneous interrogation of a large area, ensuring the maximum number of sensors receive the directly transmitted signals in every beam projection [36].

Concerning the measurement strategy, every transducer is able to function as both transmitter and receiver. The two transducers adjacent to the transmitter are disabled during measurement because of the limitation of the ultrasonic beam angle and, as such, no meaningful transmission signal will be obtained by them. As aforementioned, numbering the transducers from 1 to 16, first transducer 1 emits an ultrasonic signal and transducers 3–15 simultaneously detect the transmission signals. Then, transducer 2 is excited and transducers 4–16 are used for detection at the same time. We proceed until transducer 16 is selected as the transmitter and transducers 2–14 are selected as the receivers. So, in a whole measurement cycle, there will be 208 independent measurements, and 208 TOF values will be calculated accordingly.

3. Methods

3.1. Forward model and sensitivity matrix

The forward problem determines the theoretical output of a sensor array with specified sensor geometry and boundary setup. Usually, the forward problem can be solved by using the analytical solution.

3.1.1. CCEIT. As the frequency of CCEIT is usually hundreds of kHz, which means the signal wavelength is large enough when compared with the size of ROI, the CCEIT field can be regarded as a quasi-static electric field. The sensing area of CCEIT satisfies [29, 37]

$$\nabla \cdot ((\sigma(x,y) + j\omega\varepsilon(x,y))\nabla\phi(x,y)) = 0 \quad (x,y) \subseteq \Omega \quad (1)$$

where $\sigma(x, y)$, $\varepsilon(x, y)$ and $\phi(x, y)$ are the spatial conductivity, permittivity and potential distributions, respectively. $\omega = 2\pi f$ is the angular frequency of the excitation AC voltage source. f is the frequency of the AC voltage source. The boundary conditions are

$$\begin{cases} \phi_a(x,y) = V & (x,y) \subseteq \Gamma_a \\ \phi_b(x,y) = 0 & (x,y) \subseteq \Gamma_b \\ \partial\phi_c(x,y)/\partial\hat{n} = 0 & (x,y) \subseteq \Gamma_c, (c \neq a,b) \end{cases} \quad (2)$$

where V is the amplitude of the excitation AC voltage source. Γ_i $(i = 1, 2, \ldots, 16)$ represents the spatial locations of the 16

electrodes, $\widehat{n}$ denotes the outward unit normal vector, and a, b and c are the indexes of the excitation electrode, the detection electrode and the floating electrodes, respectively.

Sensitivity matrix of CCEIT is calculated by simulation based on the finite element method (FEM) with square elements. The ROI is created with 2601 square elements in regular grid and the relationship (sensitivity matrix) between the elements and the phase measurements are calculated with the established forward model in equations (1) and (2). The sensitivity matrix is defined as

$$S_{\mathrm{C}} = [s_{\mathrm{c}}(i,j)] = [\frac{\theta_i^j - \theta_i^0}{\sigma^1 - \sigma^0}] \tag{3}$$

where, $s_{\mathrm{c}}(i,j)$ is the sensitivity of the jth element to the ith phase measurement (i.e. with the ith electrode pair), $i = 1, 2, \ldots, 120$, $j = 1, 2, \ldots, 2601$, θ is the independent phase measurement and σ is the conductivity distribution. θ_i^0 represents the ith phase measurement when there is only background ($\sigma = \sigma^0$) inside the ROI and θ_i^j is that when the conductivity of the jth element changes to the target object ($\sigma = \sigma^1$) and the remaining elements continue as background ($\sigma = \sigma^0$).

3.1.2. UTT. Based on the assumption that ultrasonic waves propagate in a straight line, the UTT used in this work is regarded as a hard-field modality. So, the sensitivity matrix of UTT is calculated with FEM, as well, according to the same method as other hard-field modalities like x-ray tomography. The sensitivity distribution can be determined by calculating the ultrasonic energy attenuation at the position of each receiver due to obstruction in the object space [38]. For a specified transmitter and receiver, the elements will be assigned with different weights according to the size of the area inside the elements that is covered by the ultrasonic ray (i.e. the scanned area).

With a known sensor configuration, transducer beam angle and meshing parameters, a sensitivity matrix S_{U} (weight matrix) is produced [39]. First, for every ultrasonic ray, elements can be divided into two groups: the totally irrelevant elements (0 is assigned as the weights) and the intersected elements (partly/completely covered by the ray). Then, the Euclidian distances between the centre of the intersected elements and the ray are calculated. Finally, different weight values are assigned to the intersected elements on the basis of the calculated Euclidian distances. A higher weight value will be assigned to smaller distances and higher weight value means more contribution of the element in the inverse problem.

3.2. Image reconstruction

Image reconstruction is an inverse problem, which is the opposite process to forward modeling, i.e. reconstructing the component distribution inside a ROI according to the boundary measurements. In this work, time-difference imaging is used [37].

As a soft-field modality, the inverse problem of CCEIT is a difficult task to handle, which can be descibed as

$$\Delta\theta = S_{\mathrm{C}}\Delta\sigma \tag{4}$$

where $\Delta\theta$ is the time-difference phase projection vector and $\Delta\sigma$ is the relative conductivity distribution to be reconstructed. Equation (4) is a badly ill-posed problem, so some regularization methods have been introduced to solve this problem in recent decades [40, 41].

Similarly, the inverse problem of UTT can be described as

$$\Delta\tau = S_{\mathrm{U}}\Delta x \tag{5}$$

where $\Delta\tau$ is the time-difference TOF projection vector and Δx is the relative acoustic concentration distribution to be reconstructed.

In this work, an l_1-norm regularization term is introduced, and the above inverse problems are solved by the total variation (TV) algorithm [42]. The objective functions of TV algorithm for CCEIT and UTT are

$$\Delta\sigma = \arg\min_{\Delta\sigma} \frac{1}{2}\|S_{\mathrm{C}}\Delta\sigma - \Delta\theta\|^2 + \alpha\|\nabla\Delta\sigma\|_1 \tag{6}$$

$$\Delta x = \arg\min_{\Delta x} \frac{1}{2}\|S_{\mathrm{U}}\Delta x - \Delta\tau\|^2 + \beta\|\nabla\Delta x\|_1 \tag{7}$$

where α and β are the regularization parameters, ∇ is the gradient and $\|\cdot\|_1$ is the l_1-norm penalty term.

The objective function of TV regularization (equations (6) and (7)) cannot be effectively solved by traditional linearization techniques because the l_1-norm is non-differential. According to previous research, the split Bregman (SB) iterative algorithm is effective in splitting the data fidelity term and the non-differential l_1-norm penalty term to a sequence of unconstrained problems that can be easily solved. So, a SB-based TV algorithm is used in this work. Detailed description of this algorithm is available in [43, 44].

3.3. Image combination

Image combination is implemented by image fusion of the two modalities, i.e. combined images will be obtained by post-processing/combination of the normalized CCEIT images and UTT images.

The CCEIT image and UTT image will be combined pixel by pixel (element by element) according to their respective weighting coefficients, as shown in the following equation:

$$P(n) = w_{\mathrm{c}}I_{\mathrm{c}}(n) + w_{\mathrm{u}}I_{\mathrm{u}}(n) \tag{8}$$

where P is the combined image, I_{c} and I_{u} are the CCEIT image and the UTT image, $n = 1, 2, \ldots, N$, N is the size of the reshaped 1D image, and w_{c} and w_{u} are the two weighting coefficients determined by the image quality indexes. Here, three indexes of image quality are introduced to determine the coefficients: amplitude response (AR), resolution (RES) and shape deformation (SD). The definitions are as follows:

$$\mathrm{AR} = \sum I_{\mathrm{b}} \tag{9}$$

$$I_{\mathrm{b}}(i) = \begin{cases} 1, & \mathrm{abs}(I(n)) > \mathrm{abs}(\xi) \\ 0, & \text{otherwise} \end{cases} \tag{10}$$

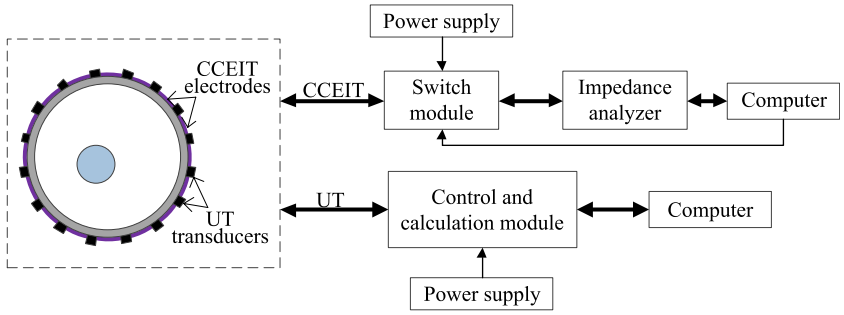

(a)

(b)

Figure 3. Experimental setup. (a) Construction. (b) Photo.

$$\xi = \gamma(\max(I) + \min(I)) \tag{11}$$

where I_b is the binary image of the reconstructed image I (i.e. I_c or I_u), ξ is the binarization threshold, and γ is the thresholding index, which defines the binarization threshold according to the maximum and minimum pixel values of the image automatically, and is set to 0.5 in this work. Then, the resolution of the image is defined as the average pixel amplitude response:

$$\mathrm{RES} = \mathrm{AR}/N. \tag{12}$$

SD is calculated on the basis of the detected objects. A new binary image S_b is first developed by making a judgment between every pixel and the detected objects (i.e. to judge if the pixel is part of the object). During this judgment, x- and y- coordinates of the centre of the detected object are obtained by searching the biggest pixel amplitudes among the object region. AR is regarded as the area of the object, so the judgment whether a pixel is part of the object can be made according to equation (13):

$$S_b(n) = \begin{cases} 1, & (X(i) - X_0)^2 + (Y(j) - Y_0)^2 < (\mathrm{AR}/\pi) \\ 0, & \text{otherwise} \end{cases} \tag{13}$$

where X_0 and Y_0 are the 2D x- and y- coordinates of the centre of the detected object and $X(i)$ and $Y(j)$ are the 2D coordinates of the pixel. $i = 1, 2, \ldots, M$. $j = 1, 2, \ldots, M$. $M \times M$ is the size of the reshaped 2D image and $N = M^2$.

Then, the two binary images I_b and S_b are compared to produce a deformation recording matrix:

$$S(n) = \begin{cases} 1, & I_b(n) \neq S_b(n) \\ 0, & \text{otherwise} \end{cases} \tag{14}$$

where $n = 1, 2, \ldots, N$.

SD is the total number of inconsistent pixels in the two images I_b and S_b:

$$\mathrm{SD} = \sum_{n=1}^{N} S(n). \tag{15}$$

Here, we have resolution of CCEIT image $\mathrm{RES_c}$, resolution of UTT image $\mathrm{RES_u}$, shape deformation of CCEIT image $\mathrm{SD_c}$ and shape deformation of UTT image $\mathrm{SD_u}$. Then the two weighting coefficients can be calculated by

$$w_c = \frac{1}{2}\left(\frac{\mathrm{RES_c}}{\mathrm{RES_c} + \mathrm{RES_u}} + \frac{\mathrm{SD_u}}{\mathrm{SD_c} + \mathrm{SD_u}}\right) \tag{16}$$

$$w_u = \frac{1}{2}\left(\frac{\mathrm{RES_u}}{\mathrm{RES_c} + \mathrm{RES_u}} + \frac{\mathrm{SD_c}}{\mathrm{SD_c} + \mathrm{SD_u}}\right) = 1 - w_c. \tag{17}$$

4. Experimental results

4.1. Experimental setup

As can be seen from figure 3, the experimental system mainly comprises a combined sensor, which includes both a 16-electrode CCEIT sensor array and a 16-transducer UT sensor array, and two separate measurement systems (one is for CCEIT and the other is for UT). The CCEIT array is mounted vertically down below the UT array, and there is a 41.5 mm gap between the two arrays.

The CCEIT measurement system consists of a power supply, a self-designed switch module, an impedance analyzer and a computer. The switch module is developed with Analog Devices ADG406 multiplexers and it can implement the whole automatic measurement cycle of CCEIT. The impedance analyzer is a Keysight E4990A Impedance Analyzer (E4990A-020, 20 Hz–20 MHz), which can provide impedance/phase measurements. The computer shows

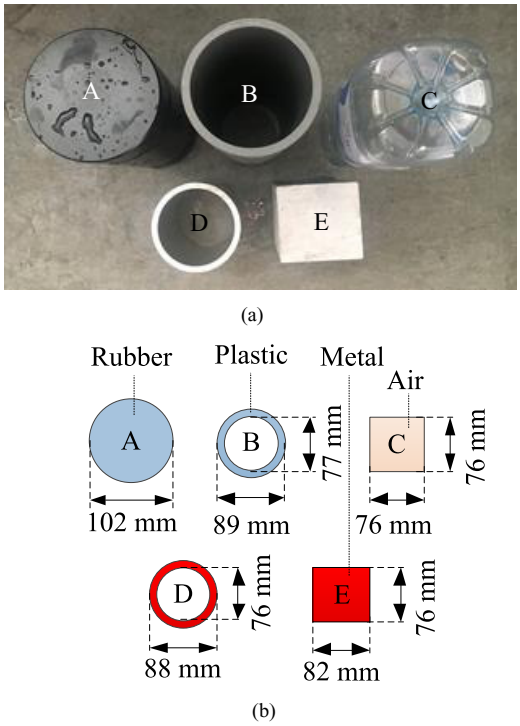

Figure 4. Experimental objects. (a) Photo. (b) Geometry.

the real-time measurement process, records the measurement data from the impedance analyzer and realizes the final image reconstruction.

The UT system includes a power supply, a self-designed control and calculation module and a computer. The power supply powers the control and calculation module. The control module controls the whole measurement process, realizes the switching process, generates and amplifies the excitation signal and deals with the received signal to obtain TOF measurements. The computer implements image reconstruction and provides the final images.

The inner and outer diameters of the tank were 288 mm and 300 mm. For the excitation frequency of CCEIT, because the measurement model includes two coupling capacitances (as can be seen from figure 1(b)), the excitation frequency should be moderately high to make the equivalent impedance of the capacitances small enough to be neglected. Based on previous research works of CCEIT/CCERT, an excitation frequency of 500 kHz is reasonable for the system and the measurement performance is good with this frequency. For the excitation frequency of UT, a moderate frequency is suitable because if the frequency is too high, the energy attenuation will be very quick during propagation (especially in a relatively big tank), and if the frequency is too low, the ultrasonic beam will be very scattered. As such, the excitation frequencies of CCEIT and UT were set to 500 kHz and 200 kHz, respectively. The outer diameter of the ultrasonic transducer was 20 mm. The sizes of the CCEIT electrodes were 49 mm (width) and 60 mm (length).

4.2. Imaging results

4.2.1. Experimental objects. Figure 4 shows a photo and the detailed geometry parameters of the experimental objects. Five objects were used in the experiments: a solid rubber rod with diameter of 102 mm (A), a plastic ring with inner and outer diameters of, respectively, 77 mm and 89 mm (B), a square-shaped empty bottle with a base side of 76 mm (C), a metal ring with inner and outer diameters of 76 mm and 88 mm, respectively (D), and a solid metal block with a base parameter of 82 mm (length) and 76 mm (width) (E). Based on these objects, six setups, named S1–S6, were tested during the experiments.

4.2.2. Imaging results and image combination. Table 1 shows the reconstructed images of CCEIT and UTT. It is obvious that UTT is more sensitive to the shape of the object, which is especially clear for setup S1. Again, UTT is more accurate in reconstructing the position information, especially for the central area of the tank. As mentioned in section 1, CCEIT and UT are sensitive to different properties, which is verified by the reconstructed images of S5 and S6. The two objects in S5 are both solid rings, so UTT cannot differentiate them. However, the two rings have different electrical properties: one is conductive and the other is not, so showing the difference between them is an easy task for CCEIT. In contrast, the two objects in S6 have different acoustic impedances (one is gas and the other is solid) but are both non-conductive, so UTT can perfectly indicate their difference but CCEIT cannot. It is interesting to note that UTT tries to establish the shape of the ring in S5.

Table 2 shows the image quality indexes and the corresponding weighting coefficients of the images in table 1. It is found that the resolution of images obtained by CCEIT is overall higher than that obtained by UTT, while standard deformation of images obtained by UTT is overall smaller than that obtained by CCEIT. That makes the weighting coefficients of most setups around half and half for image combination.

The last column of table 1 shows the combination results of CCEIT images and UTT images, which verifies the feasibility of combining the two contactless modalities. By introducing a judgement strategy, noises that exist in only one of the two images (one is a CCEIT image and the other is an UTT image) are removed. So, the combined images can have better noise immunity and show good complementary characteristics of the CCEIT and UTT images. This means systematic errors in the two systems can be effectively removed so long as they do not exist at the same place. By effective combination, this dual-modality system has the ability to contactlessly differentiate both the electrical property and acoustic property of the sensing area. Further, the combined images show good position information of the objects but cannot provide good shape information. So, more combination methods need to be undertaken for further shape reconstruction.

Table 1. Reconstructed images and combination results.

Setups	CCEIT	UTT	Combined image
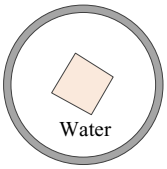 S1	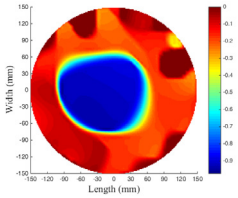	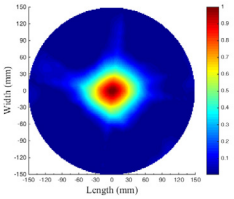	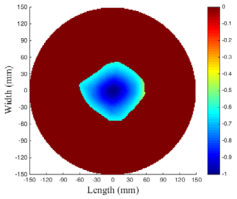
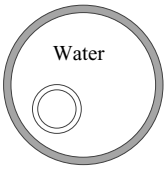 S2	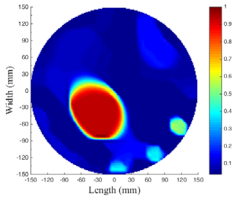	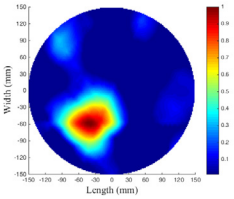	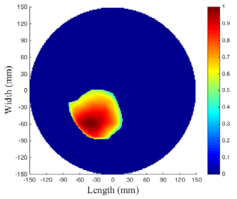
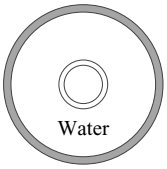 S3	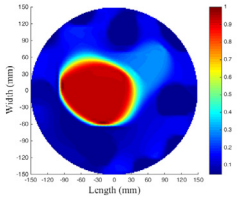	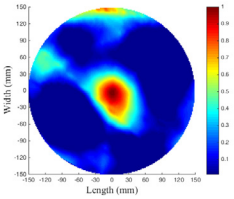	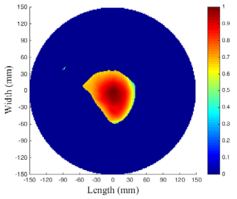
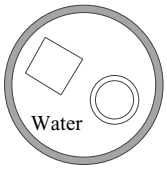 S4	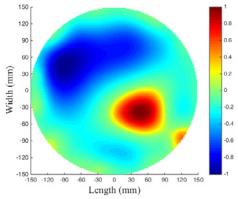	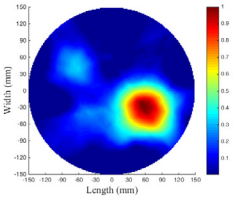	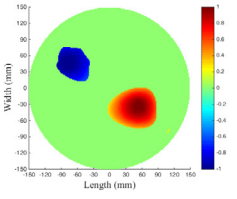
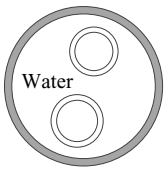 S5	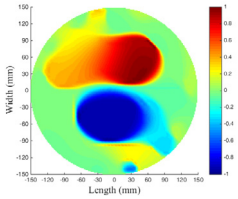	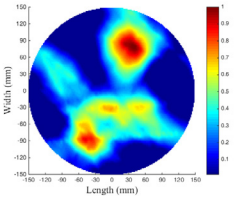	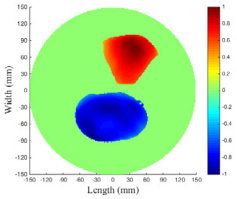
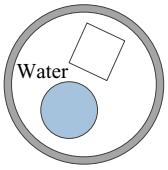 S6	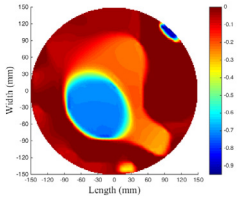	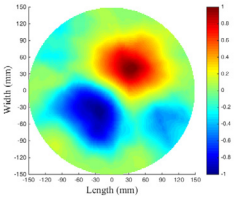	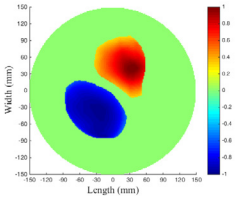

Table 2. Image quality indexes of the reconstructed images.

Setups	Sensor	RES	SD	*w*
S1	CCEIT	0.1862	43	0.502
	UTT	0.0122	3	0.498
S2	CCEIT	0.0512	15	0.417
	UTT	0.054	8	0.583
S3	CCEIT	0.1133	39	0.520
	UTT	0.0143	7	0.480
S4	CCEIT	0.1495	438	0.496
	UTT	0.0191	52	0.504
S5	CCEIT	0.1104	421	0.446
	UTT	0.1259	312	0.554
S6	CCEIT	0.09	53	0.666
	UTT	0.0838	234	0.334

5. Discussion

The demonstrated results here show the performances of two contactless tomography techniques, CCEIT and UTT, and of preliminarily combining the two modalities by image post-processing. The separate imaging results are good overall and the two modalities show different advantages as well as limitations. This section serves to analyze the current limitations and discuss possible improvements of the combined system. Besides, the novelty and advantages of the proposed combination are highlighted.

In our previous research, CCEIT has shown good performance and potential in both industrial and biomedical applications [36, 45]. Images obtained by CCEIT are as good as those obtained by traditional contact EIT. But in this work, the performance of CCEIT is not very satisfactory, especially in imaging of objects positioned in the central area of the ROI. Besides, the reconstructed positions for the objects near the tank wall show obvious distortion (the reconstructed positions are closer to the centre when compared with the actual positions). The explanations are listed as follows, mainly focusing on the limitations of CCEIT and the experimental setup. First, the tank wall is too thick to ensure good CCEIT performance. According to the principle of capacitively coupled measurement, the two coupling capacitances formed by the insulating tank wall are the key to the CCEIT technique. Although they make contactless measurement possible, they present an unfavorable background signal. The impedance of the ROI is the actual part of interest, so the insulating wall is required to be as thin as possible to make the equivalent impedance of the capacitances small enough to be neglected. Second, the excitation signal of CCEIT is too weak to obtain a good measurement signal. The excitation signal of CCEIT is provided by the impedance analyzer with a maximum amplitude of 1 V, which is much smaller when compared with the excitation signal of UTT (12 V). In further studies, a specific hardware system for CCEIT should be developed to overcome this limitation. Third, the size of the tank is relatively too large for ET, especially when the excitation signal is weak. In this case, the electrical signal is very weak in the central area, which is why most EIT-related applications focus on a limited-size ROI. Rather, measuring large-scale tanks/pipes is one of the main advantages of ultrasonic-related methods (both in flow-rate measurement, ranging and tomography) and this is more outstanding when it comes to TOF measurement. So, the scale of applications should be considered to exploit the advantages of combining CCEIT and UTT to the full, and more suitable experimental setups should be developed for further study. In addition, whether the two sensor arrays will have an influence on each other's performance, and how extensive this influence might be, are not taken into consideration in this work. Although the two sensor arrays can work effectively with the current setup and no significant interplay between them can be observed, further research work needs to be carried out to investigate the exact amount of interplay between the two arrays and to optimize the configuration of the combined sensor.

UTT has better overall performance according to the images, but we can also observe its deficiency. First, the UTT system is not sensitive enough to the shape information of objects near the boundary: this can be observed in setups where there is enough space between the object and the boundary. Second, the UTT failed to provide a good image in some cases when there is more than one object in the ROI. These two problems can be improved by adding more ultrasonic transducers. In the UTT method, a large number of ultrasonic transducers are necessary to obtain a good spatial resolution. By updating the 16-transducer sensor array to a 32-transducer one, or even a 64-transducer one, the blind area near the boundary will be smaller and the spatial resolution of measurement will effectively be improved. Of course, a trade-off between measurement resolution and system complexity should be taken into consideration at the same time.

This work bridges the novel CCEIT and UT modalities together to provide a new meaningful method of contactless imaging, which retains the advantages of both modalities and is promising in a broad range of applications.

6. Conclusion

As a novel contactless EIT technique, CCEIT has not been compared with other modalities or yet involved in multi-modal systems. This work investigates two contactless tomography techniques, CCEIT and UT, and shows their correlation and complementarity by comparison and combination of separately reconstructed images. A sensor, combining a 16-electrode CCEIT sensor array and a 16-transducer UT sensor array, was developed and two corresponding measurement systems were developed. Experimental results show that both modalities can provide useful images through non-invasive and non-intrusive measurement. The combination results with image fusion shows a great potential for this new dual-modality imaging for material characterization in liquid media. The contactless nature of this multi-modality imaging makes it a great candidate for use in harsh process environments, where

contact with the materials under test and access to the process vessels are prohibited.

Acknowledgments

The authors would like to acknowledge financial support from the China Scholarship Council (CSC) (Grant No. 201706320268). The contributions of Paul Hetherington in developing the UT hardware system and Carl Chittenden in developing the software of the CCEIT switching module are also gratefully acknowledged.

ORCID iDs

Yandan Jiang https://orcid.org/0000-0002-1677-4671
Manuchehr Soleimani https://orcid.org/0000-0002-6341-9592
Baoliang Wang https://orcid.org/0000-0002-0045-0576

References

[1] Becky M S and Williams R A 1996 Process tomography: a European innovation and its applications *Meas. Sci. Technol.* **7** 215–24
[2] York T 2001 Status of electrical tomography in industrial applications *Proc. SPIE* **4188** 175
[3] Wahab Y L *et al* 2015 Non-invasive process tomography in chemical mixtures—a review *Sens. Actuators* B **210** 602–17
[4] Zhang R H *et al* 2014 Data fusion in dual-mode tomography for imaging oil–gas two-phase flow *Flow Meas. Instrum.* **37** 1–17
[5] Qiu C, Hoyle B S and Podd F J W 2007 Engineering and application of a dual-modality process tomography system *Flow Meas. Instrum.* **18** 247–54
[6] Sun J T and Yang W Q 2015 A dual-modality electrical tomography sensor for measurement of gas–oil–water stratified flows *Measurement* **66** 150–60
[7] Lionheart W R B 2004 EIT reconstruction algorithms: pitfalls, challenges and recent developments *Physiol. Meas.* **25** 125–42
[8] Tapp H S *et al* 2003 Chemical engineering applications of electrical process tomography *Sens. Actuators* B **92** 17–24
[9] Holder D S 2004 *Electrical Impedance Tomography: Methods, History and Applications* (Boca Raton, FL: CRC Press)
[10] Brown B H 2001 Medical impedance tomography and process impedance tomography: a brief review *Meas. Sci. Technol.* **12** 991–6
[11] Kanti B T 2018 Applications of electrical impedance tomography (EIT): a short review *IOP Conf. Ser.: Mater. Sci. Eng.* **331** 012004
[12] Seo J K *et al* 2008 Frequency-difference electrical impedance tomography (fdEIT): algorithm development and feasibility study *Physiol. Meas.* **29** 929–44
[13] Cao Z, Wang H X and Xu L J 2008 Electrical impedance tomography with an optimized calculable square sensor *Rev. Sci. Instrum.* **79** 103710
[14] Booth M J and Basarab-Horwath I 2002 Comparing electrode configurations for electrical impedance tomography *Electron. Lett.* **32** 648–9
[15] Wei K, Qiu C H and Primrose K 2016 Super-sensing technology: industrial applications and future challenges of electrical tomography *Phil. Trans. R. Soc.* A **374** 20150328
[16] Hoyle B S 1996 Process tomography using ultrasonic sensors *Meas. Sci. Technol.* **7** 272–80
[17] Goh C L *et al* 2017 Ultrasonic tomography system for flow monitoring: a review *IEEE Sens. J.* **17** 5382–90
[18] Rahiman M H F *et al* 2006 Ultrasonic transmission-mode tomography imaging for liquid/gas two-phase flow *IEEE Sens. J.* **6** 1706–15
[19] Wahab Y A *et al* 2011 Application of transmission-mode ultrasonic tomography to identify multiphase flow regime *Int. Conf. on Electrical, Control and Computer Engineering* pp 119–23
[20] Nor Ayob N M *et al* 2010 Improving gas component detection of an ultrasonic tomography system for monitoring liquid/gas flow *6th Int. Colloquium on Signal Processing & Its Applications* pp 278–82
[21] Soleimani M 2006 Electrical impedance tomography imaging using *a priori* ultrasound data *Biomed. Eng. Online* **5** 8
[22] Yunus F R M *et al* 2014 Simulation study of electrode size in air-bubble detection for dual-mode integrated electrical resistance and ultrasonic transmission tomography *Powder Technol.* **256** 224–32
[23] Samir T and Mahmoud M 2015 A multimodal image reconstruction method using ultrasonic waves and electrical resistance tomography *IEEE Trans. Imaging Process.* **24** 3512–21
[24] Steiner G *et al* 2007 Tomographic image reconstruction from dual modality ultrasound and electrical impedance data *IFMBE Proc.* **17** 288–91
[25] Ain K *et al* 2017 Dual modality electrical impedance and ultrasound reflection tomography to improve image quality *J. Electr. Bioimpedance* **8** 3–10
[26] Tan C *et al* 2016 Oil–water two-phase flow measurement with combined ultrasonic transducer and electrical sensors *Meas. Sci. Technol.* **27** 125307
[27] Liang G H, Ren S J and Dong F 2017 Ultrasound guided electrical impedance tomography for 2D free-interface reconstruction *Meas. Sci. Technol.* **28** 074003
[28] Hoyle B S *et al* 2001 Design and application of a multi-modal process tomography system *Meas. Sci. Technol.* **12** 1157–65
[29] Wang B L *et al* 2013 A novel electrical resistance tomography system based on C4D technique *IEEE Trans. Instrum. Meas.* **62** 1017–24
[30] Wang B L *et al* 2013 Modeling and optimal design of sensor for capacitively coupled electrical resistance tomography system *Flow Meas. Instrum.* **31** 3–9
[31] Zhang M and Soleimani M 2016 Simultaneous reconstruction of permittivity and conductivity using multi-frequency admittance measurement in electrical capacitance tomography *Meas. Sci. Technol.* **27** 025405
[32] Yao J and Takei M 2017 Application of process tomography to multiphase flow measurement in industrial and biomedical fields-a review *IEEE Sens. J.* **17** 8196–205
[33] Jiang Y D and Soleimani M 2018 Capacitively coupled phase-based dielectric spectroscopy tomography *Sci. Rep.* **8** 17526
[34] Jiřík R *et al* 2012 Sound-speed image reconstruction in sparse-aperture 3D ultrasound ransmission tomography *IEEE Trans. Ultrason. Ferroelectr. Freq. Control* **59** 254–64
[35] Rahiman M H F *et al* 2012 Design and development of ultrasonic process tomography *Ultrasonic Waves* (Rijeka: InTech) pp 211–26
[36] Rahiman M H F *et al* 2014 An investigation on chemical bubble column using ultrasonic tomography for imaging of gas profiles *Sens. Actuators* B **202** 46–52
[37] Jiang Y D and Soleimani M 2018 Capacitively coupled resistivity imaging for biomaterial and biomedical applications *IEEE Access* **6** 27069–79

[38] Rahiman M H F *et al* 2012 Ultrasonic tomography—image reconstruction algorithms *Int. J. Innovat. Comput. Inf. Control* **8** 527–38
[39] Koulountzios P, Rymarczyk T and Soleimani M 2018 Ultrasonic tomography for automated material inspection in liquid masses *9th World Congress on Industrial Process Tomography* pp 693–702
[40] Cui Z Q *et al* 2016 A review on image reconstruction algorithms for electrical capacitance/resistance tomography *Sensor Rev.* **36** 429–45
[41] Peng L H, Merkus H and Scarlett B 2000 Using regularization methods for image reconstruction of electrical capacitance tomography *Part. Part. Syst. Charact.* **17** 96–104
[42] Goldstein T and Osher S 2009 The split Bregman method for L1-regularized problems *SIAM J. Imaging Sci.* **2** 323–43
[43] Li F *et al* 2017 Total variation regularization with split Bregman-based method in magnetic induction tomography using experimental data *IEEE Sens. J.* **17** 976–85
[44] Borsic A *et al* 2010 *In vivo* impedance imaging with total variation regularization *IEEE Trans. Med. Imaging* **29** 44–54
[45] Jiang Y D and Soleimani M 2018 Capacitively coupled impedance imaging based on wideband phase measurement *9th World Congress on Industrial Process Tomography* pp 3–9